Published in final edited form as:
Nat Struct Mol Biol. 2017 April ; 24(4): 414–418. doi:10.1038/nsmb.3386.

Cryo-EM structure of a separase-securin complex at near-atomic resolution

Andreas Boland[1], **Thomas G. Martin**[1], **Ziguo Zhang**[1], **Jing Yang**[1], **Xiao-chen Bai**[1], **Leifu Chang**[1], **Sjors H.W. Scheres**[1], and **David Barford**[1]

[1]MRC Laboratory of Molecular Biology, Francis Crick Avenue, Cambridge, CB2 0QH, UK

Abstract

Separase is a caspase-family protease that initiates chromatid segregation by cleaving the kleisin subunits (Scc1 and Rec8) of cohesin, and regulates centrosome duplication and mitotic spindle function through cleavage of kendrin and Slk19. To understand the mechanisms of separase regulation by securin we used single particle cryo-EM to determine a near-atomic resolution structure of the *C. elegans* separase-securin complex. Separase adopts a triangular-shaped bilobal architecture comprising an N-terminal tetratricopeptide repeat (TPR)-like α-solenoid domain docked onto the conserved C-terminal protease domain. Securin engages separase in an extended antiparallel conformation interacting with both lobes. It inhibits separase by interacting with the catalytic site through a pseudo-substrate mechanism, revealing that in the inhibited separase-securin complex, the catalytic site adopts a conformation compatible with substrate binding. Securin is protected from cleavage because an aliphatic side-chain at the P1 position represses protease activity by disrupting the organization of catalytic site residues.

Introduction

The coordinated and accurate segregation of paired chromatids is critical to somatic cell division in mitosis and the genesis of germ cells in meiosis. Timely disjunction of coherent chromatids is achieved through removal of centromeric cohesin mediated by the separase-catalysed proteolysis of the kleisin subunit of cohesin complexes 1–3. Accurate chromatid disjunction is crucial to prevent chromosome missegregation that contributes to aneuploidy and tumourigenesis 4,5. To ensure genome stability, separase activity is tightly regulated by

Correspondence should be addressed to A.B. and D.B. (aboland@mrc-lmb.cam.ac.uk and dbarford@mrc-lmb.cam.ac.uk).

Author contributions. Z.Z. cloned the separase-securin constructs used in this study. A.B. and J.Y. generated the wild-type and mutant separase-securin viruses, respectively. A.B. established the protein purifications. A.B. and T.G.M. prepared grids and collected EM data with contributions from X-C.B. and L.C. A.B. analysed EM data and determined the 3D reconstructions aided by T.G.M. A.B. and D.B. built the model *ab initio* and made the figures. D.B. directed the project and designed experiments with A.B. A.B. and D.B. wrote the manuscript with input from all other authors.

Competing Financial Interests. The authors declare no competing financial interests.

Accession codes. EM maps for the *C. elegans* and *H. sapiens* data sets are deposited with the EM-DB with accession codes: 3583 and 3584 respectively. Protein coordinates of separase-securin are deposited with RCSB with PDB code: 5MZ6.

Data availability. EM maps for the *C. elegans* and *H. sapiens* data sets are deposited with the EM-DB with accession codes: 3583 and 3584 respectively. Protein coordinates of separase-securin are deposited with RCSB with PDB code: 5MZ6. Source Data files and materials related to this paper are available on request.

Europe PMC Funders Author Manuscripts

binding to its inhibitory chaperone securin 6–8, a natively unfolded protein 9,10 that is present in excess over separase in the cell and associates with separase during translation 6–8,11. Paradoxically, in addition to its inhibitory function, securin plays an important role in promoting separase activity 12–14. This likely results from stabilizing effects, since securin deficient human HCT116 cells exhibit a roughly four-fold reduction in separase levels 12 and conversely, overexpression of separase results in elevated levels of securin 15. Stabilizing effects of securin are also observed in other species including the separase-securin complex from *Caenorhabditis elegans* 16. In vertebrates a small proportion is also inhibited through CDK-cyclin B1-dependent phosphorylation and binding 15,17,18. Separase activation is triggered by the anaphase-promoting complex (APC/C)-dependent ubiquitin-mediated proteolysis of securin and cyclin B1 (refs 19–21).

Separase is a caspase-family protease comprising a C-terminal separase protease domain (SPD) with specificity for cleaving substrates C-terminal to an Arg residue (P1) within an (S/D)xExxR motif 3,7,22. In budding yeast, polo kinase-dependent phosphorylation of Scc1 (Pds1) at the Ser residue at P6 regulates Scc1 cleavage and thus sister chromatid separation 23. A large N-terminal domain contributes to securin and substrate interactions 14,22,24. Crystallographic studies of the separase protease domain (SPD) with inhibitory peptides explained the basis for substrate selection 25, however the molecular mechanisms underlying separase regulation have not yet been defined. To understand the dual mechanisms of activation and repression of separase activity by securin we used single particle cryo-EM to determine a near-atomic resolution structure of the *C. elegans* separase-securin complex. We also determined a medium resolution reconstruction of the human separase-securin complex, revealing the evolutionary conservation of separase's triangular shape.

This study provides insights into the overall architecture of separase, explains the substrate-occlusion inhibitory mechanism of securin and rationalizes the strict necessity of an arginine residue in the P1 binding pocket to mediate substrate-assisted cleavage. We also demonstrate the applicability of cryo-EM to resolve structures of macromolecules of ~150 kDa that are difficult to crystallize.

Results

Cryo-EM structure of a separase-securin complex at 3.8 Å resolution

To optimize the contrast of a relatively small complex in cryo-electron micrographs, and to overcome preferred molecule orientations of this complex encountered in vitreous ice, we used graphene oxide coated EM grids 26 (Supplementary Fig. 1). We determined a reconstruction of the asymmetric separase-securin complex at 3.8 Å resolution (Fig. 1 and Supplementary Figs 1 and 2). Most of the complex, particularly the larger separase subunit, was well defined in EM density. Side-chain density was unambiguously assigned for more than 95% of all structured amino acid allowing complete *ab initio* model building of separase. Securin, which forms an extended structure that interacts mainly with the periphery of separase, was well resolved around the substrate-binding site but less well-defined elsewhere (Supplementary Fig. 2 and Table 1).

Overall architecture of the *C. elegans* separase-securin complex

The *C. elegans* separase-securin adopts a triangular-shaped bilobal architecture, measuring 110 Å in its longest dimension and about 70 Å in its two other dimensions. Separase is composed of an N-terminal α-solenoid domain adjoined to the C-terminal separase protease domain (SPD) 25 (Fig. 1). A clearly defined cleft is situated at the interface of these two domains. The α-solenoid domain comprises 25 α-helices, mainly arranged as a right-handed superhelix that resembles a tetratricopeptide repeat (TPR) superhelix, as predicted 27. Compared to a canonical TPR superhelix however, compression of the helix and the irregular length of its constituent α-helices create a compact globular structure lacking the deep surface grooves typical of TPR proteins (Supplementary Fig. 3). The C-terminus of the α-solenoid interacts with the SPD, whereas its N-terminus is capped by securin, possibly explaining how securin contributes to separase stability 12–14 (Figs 1b and 2a). The α-solenoid domain accommodates two disordered insertions. Insert-1 includes the site of regulatory CDK-phosphorylation of human separase 17,28, whereas insert-2 incorporates the auto-cleavage sites 2,29,30 and cyclin B1 (refs 15,18) and PP2A 31 binding sites of vertebrate separase (Fig. 1 and Supplementary Fig. 4). Both inserts project towards the separase catalytic site, located within reach of the tips of both inserts (Fig. 1b and Supplementary Fig. 4a, b). Insert-2 of human separase is markedly longer than its counterpart in *C. elegans* separase, such that all three auto-cleavage sites are accessible to the catalytic site. The marked positive electrostatic potential on one surface of separase (Fig. 1c) might be related to its activation by DNA 32 and the stimulation of Rec8 cleavage in meiosis by multisite phosphorylation of Rec8, facilitating high affinity binding of the substrate 27.

The SPD of *C. elegans* separase, like *Chaetomium thermophilum* SPD (*Ct*SPD) 25, is divided into two sub-domains, one of which is the C-terminal active protease domain (APD) (Fig. 1a, b and Supplementary Fig. 5). APD belongs to the caspase/gingipain family of cysteine proteases and incorporates an essential Cys-His catalytic dyad 1,17,33. The APD comprises a central β-sheet flanked on both sides by α-helices (Fig. 1b). The adjacent pseudoprotease domain (PPD) extends the APD β-sheet, reminiscent of the architecture of caspase dimers formed from active and inactive catalytic subunits 33. An α-helical insertion within the PPD stretches out over the PPD and APD, forming extensive contacts with the APD (Fig. 1b, right panel). This long α-helical insertion is indispensible for protease activity, presumably due to its roles in substrate recognition, as discussed below, and in contributing to the structural integrity of the protein 25. It is followed by a four-helix bundle, which forms at the periphery of the APD (Fig. 1b, left panel).

Loop L4 conformation is constrained in the full-length protein

The SPD of the *C. elegans* separase-securin complex and *Ct*SPD 25 superimpose closely with an RMSD of 3.5 Å over 365 Cα-atoms and 1.6 Å over 121 Cα-atoms for the APD (Supplementary Fig. 5). The four-helix bundle is shifted in the *C. elegans* structure towards the N-terminus of the molecule by 9 Å and rotated by 7°. His1014^{Sep} and Cys1040^{Sep} of the catalytic dyad are located in loops L3 and L4, respectively (separase and securin residues are denoted with superscript ‘Sep’ and ‘Sec’). Caspases are regulated by the conformation of the L4 loop 33, and in the context of the securin-separase complex, the L4 loop adopts an active

conformation, although the position of its tip differs from its counterpart in *Ct*SPD 25 (Fig. 2d).

The C-terminus of the α-solenoid domain is capped by the SPD. An extensive hydrophobic interface is created primarily by the H23 and H24 α-helices of the α-solenoid docking onto the central β-sheet of the PPD (Fig. 1b). Its large size suggests a stable interaction. The tip of the L4 loop projects into the groove of the α-solenoid superhelix (Fig. 2a, b). Phe1052^{Sep}, a conserved hydrophobic residue in separase (Supplementary Fig. 6), is located at the tip of L4 and is buried within a hydrophobic pocket of the α-solenoid domain (Fig. 2c). Mutations of the L4 loop in *Ct*SPD modulate Scc1 cleavage rates 25, showing that the conformation of the L4 loop contributes slightly to catalytic activity.

Securin acts as a non-cleavable pseudo-substrate

Securin is an intrinsically disordered protein 9,10 that functions as an inhibitory chaperone to both stabilize separase 12–14, and through a pseudo-substrate mechanism, inhibit protease activity 14,29. Our structure shows that bound to separase, securin forms an extended conformation interacting along the entire length of separase in an anti-parallel orientation (Fig. 1b, c). The N-terminal 116 residues, including the APC/C degron recognition and ubiquitination sites are unstructured (Fig. 1a). The separase-binding motif (SBM) encompasses residues 118-199 and is part of a previously identified inhibitory segment of securin 34 that is evolutionarily well conserved (Supplementary Fig. 7). The N-terminus of the SBM blocks the separase catalytic site filling a 16 Å-wide cleft between the α-solenoid domain and the SPD (Figs 1 and 2c). SBM's C-terminus curls along a hydrophobic path on the outside of the α-solenoid domain, with two short α-helices anchored within adjacent hydrophobic grooves (Figs 1b, c and 2a). This is in agreement with biochemical studies indicating that the C-terminus of securin contacts the α-solenoid domain of separase 14,24. A C-terminal fragment of the Scc1 substrate remains bound to separase even in the absence of the cleavage site residues 22, indicating the importance of the N-terminal α-solenoid domain in conferring high affinity binding to both substrate and inhibitor.

Separase substrates share a common [D/E/S]xExxR motif (positions P6 to P1), and are cleaved immediately C-terminal to the P1 Arg residue 3,7,22 (Supplementary Fig. 7). Polo kinase-phosphorylation of yeast Scc1 at the P6 serine stimulates separase cleavage 23. A DIExxΦ motif in securin mimics substrate recognition with the P1 Arg substituted by a hydrophobic residue (Met126^{Sec} in *C. elegans* securin) 34 (Supplementary Fig. 7). Notably, the P1 Arg of separase substrates is critical for cleavage 7,22,35–37. Replacing Arg with Ala, Asp or Glu eliminates proteolysis 3,7,13,22, whereas conversely the securin pseudo-substrate motif is cleaved when an Arg is substituted for the hydrophobic residue at its P1-binding pocket 25,34.

Our structure reveals that the mode of interaction of the securin pseudo-substrate motif with *Ce* separase is remarkably similar to the interactions between the *Ct*SPD and a covalently linked peptide mimicking Scc1 (Fig. 3a, b and Supplementary Fig. 8) 25. This confirms the concept that securin acts as a pseudo-substrate inhibitor 14,29,34, and importantly indicates that in the inhibited *Ce* separase-securin complex, the separase catalytic site architecture

adopts a conformation compatible with substrate recognition. In the *Ce* separase-securin complex, Ile122^{Sec} (P5) forms hydrophobic interactions with Phe783^{Sep}, a strictly conserved aromatic residue of the α-helical insert (Fig. 3c and Supplementary Fig. 6). This interaction rationalizes the strong conservation of residues with non-polar character at the P5 site of separase substrates (Supplementary Fig. 7). Glu123^{Sec} at P4 forms electrostatic interactions with the highly conserved Arg1083^{Sep}, mimicking Scc1-*Ct*SPD interactions 25. Amino acid side chains at variable positions P3 and P1' (ref. 22) are solvent exposed. C-terminal to the pseudo-substrate motif, securin inserts into the cleft separating the SPD and α-solenoid domain, contacting the L4 loop (Fig. 2a, c).

Similarly to the P1 Arg of the Scc1-peptide bound to *Ct*SPD 25, Met126^{Sec} is anchored by the P1-binding pocket of *Ce* separase (Fig. 3c-e). This deep pocket is lined by a mixture of conserved hydrophobic and polar residues including His1014^{Sep} of the catalytic dyad (Supplementary Fig. 6). Through conformational flexibility, the P1 pocket accommodates both non-polar residues of securin and the P1 Arg residue of separase substrates (Fig. 3d, e and Supplementary Video 1). Importantly, the interactions of an Arg side chain at the P1 pocket organize the configuration of catalytic site residues required for peptide cleavage. In the *Ct*SPD structure, the invariant Asp2151 residue, equivalent to Asp1082^{Sep} that is rotated out of the P1-binding pocket in *Ce* separase, forms a stable bi-dentate salt-bridge with the substrate P1 Arg guanidinium group 25 (Fig. 3e). This interaction allows the Nε atom of the P1 Arg guanidinium group to donate a hydrogen bond to the main chain carbonyl of Gly2082^{Sep} that orients the catalytic His2083^{Sep} side chain to create the oxyanion hole for the carbonyl oxygen at P1 (Fig. 3e). In the *Ce* separase-securin complex, the P1-binding pocket widens to accommodate the non-polar Met126^{Sec} side chain. Relative to their counterparts in *Ct*SPD, Gly1013^{Sep} and the imidazole ring of His1014^{Sep} move away from Met126^{Sec} by almost 2 Å (Fig. 3d and Supplementary Fig. 8a versus b). Thus, an Arg at P1 functions to mediate catalysis by orienting the catalytic His to create the oxyanion hole, necessary for cleavage of the scissile bond 1,17.

The triangular shape of separase is conserved throughout evolution

Although the SPD is conserved across eukaryotes (Supplementary Fig. 5), sequence similarities within the α-solenoid domain are difficult to discern (Supplementary Fig. 4c). However, the triangular shape of separase-securin is evolutionarily conserved because the structure of *C. elegans* separase-securin is similar to a medium resolution cryo-EM reconstruction of human complex we determined (Fig. 4a, b and Supplementary Fig 1), and consistent with a previous negative stain EM reconstruction 24. *C. elegans* separase-securin resembles the 'whale'-like domain described in the human separase-securin structure 24. The flexible 'tail'-like feature at the N-terminus of human separase-securin is not present in our structure of the *C. elegans* complex. This likely represents the N-terminal 650 residues of human separase 27 absent from *C. elegans* (Supplementary Fig. 4). A recently reported EM structure of *C. elegans* separase-securin complex at 24 Å resolution 16 revealed a bi-lobal architecture that has similar overall dimensions and is generally compatible with our cryo-EM structure, despite the lower resolution and use of negative stain.

Discussion

The role of the substrate Arg P1 residue that participates in organizing the catalytic site is reminiscent of other enzymes that derive specificity through substrate-assisted catalysis 38,39. It explains the requirement for an Arg at P1 for substrate cleavage 3,7,22 and why securin is capable of engaging the separase substrate-binding site, competing with Scc1, without itself being cleaved 22. Thus, securin inhibits separase through a competitive mechanism that interferes with substrate recognition, and represses its intrinsic protease activity through small conformational rearrangements of its catalytic site. This inhibition mechanism contrasts with XIAP inhibition of caspases which block access to the substrate-binding cleft by binding in the reverse orientation 40,41.

Here we reveal how securin inhibits separase through a substrate occlusion mechanism. Additionally, securin destruction and its displacement from the TPR lobe may promote a conformational change of separase affecting the catalytic site and L4 loop that stimulates catalytic activity. Future structural studies of securin-free separase are required to address this question and also to understand other regulatory mechanisms including the mutually exclusive CDK1-cyclin B1 dependent repression of vertebrate separase that involves a phospho-dependent Pin1-catalysed peptidyl prolyl *cis/trans*-isomerization 28 leading to cyclin B1 association and separase inhibition.

Mutations, overexpression or mislocalization of separase leads to elevated tumour development 42,43, and hence inhibition of separase is a tempting pharmacological target. This structure will provide a rational molecular basis for the design of small molecule drug targets to inhibit uncontrolled separase activity in certain cancer types.

Online Methods

Cloning and expression of *Caenorabditis elegans* and *Homo sapiens* separase-securin complex genes

The cDNAs encoding for the *Caenorabditis elegans*, *Homo sapiens* and *Chaetomium thermophilum* separase and securin genes were ordered as gene optimized versions for expression in insect cells, and synthesized cDNAs (GeneArts /Thermo Fisher) were subsequently cloned into pU1 (separase) and pF1 (securin) vectors 44. A double StrepII-tag followed by a TEV (tobacco etch virus) site was fused N-terminal of the separase gene. An N-terminal truncation of 139 residues of *Ce* securin was generated using mutagenesis PCR, and a TEV-cleavable MBP tag was added C-terminal to securin in the human construct. *Chaetomium thermophilum* separase and the *C. thermophilum* separase-securin complex were generated with the auto-cleavage site E1643R/R1646E mutant in separase. A *C. thermophilum* separase-securin complex with an N-terminal 180 residue truncation of securin was generated by mutagenesis PCR. The resultant plasmids were transformed into MultiBacDH10α cre cells to generate bacmids through *in vivo* recombination 44. A single recombinant vector was used for recombinant baculovirus generation.

Separase-securin overexpression

Recombinant P3 baculoviruses were used for infection of High Five insect cells (Invitrogen) at a cell density of roughly 2.0 x 10^6 cells per ml. The cells were incubated for 72 hours at 27 °C at 150 rev./min, harvested at a cell viability rate of ~80%, flash-frozen in liquid nitrogen and stored at -80 °C.

Purification of separase-securin complexes

Purification of the protein complexes were performed at 4 °C. Cells were resuspended in lysis buffer [50 mM Tris/HCl (pH 8.3), 250 mM NaCl, 1 mM EDTA, 1 mM DTT, Protease inhibitor cocktail tablets (PIC) (Complete EDTA-free; Roche Diagnostics GmbH), 0.1 mM PMSF, 5 units/ml benzonase (Novagen)], subsequently sonicated and centrifuged for 1 h at 48,000 g. The soluble fraction was slowly (1 ml/min flow rate) applied to a 5 ml StrepTactin Superflow Cartridge (Qiagen) and washed with wash buffer (lysis buffer without PIC, PMSF and benzonase) until stable UV absorption could be observed. Peak fractions were incubated with TEV protease at 4 °C overnight and wash buffer without NaCl (buffer A) was used for a two-fold dilution before loading onto a ResourceQ anion-exchange column (GE Healthcare) the next day. After a washing step the complexes were eluted using a gradient with buffer B [20 mM Tris/HCl (pH 8.0), 1 M NaCl, 1 mM DTT]. A final size exclusion step on a Superose 6 Increase 10/300 GL column with 20 mM Hepes-NaOH (pH 7.8), 200 mM NaCl and 1 mM DTT was performed.

Preparation of graphene oxide support covered grids

Graphene oxide dispersion (Sigma-Aldrich; 2 mg/mL in H_2O) was diluted ten-fold with ddH_2O to a final concentration of 0.2 mg/ml and subsequently spun down at 300g for ~15 sec to remove large aggregates of graphene oxide flakes (pellet formation could be observed occasionally) [as described in 26]. After incubation for one minute with graphene oxide dispersion, Quantifoil grids were glow discharged for one minute utilizing a Edwards Sputter Coater S150B. After incubation the graphene oxide solution was removed by blotting briefly with Whatman No.1 filter paper and washed by absorbing 20 µl ddH_2O onto the graphene oxide coated side twice and once on the back side of the grid with blotting steps in between (for detailed video and protocol see https://figshare.com/articles/Graphene_Oxide_Grid_Preparation/3178669). The tendency of biological molecules to adopt preferred orientations in thin vitreous ice likely results from interactions at the hydrophobic air-water interface. Presumably these interactions favour the largest exposed hydrophobic surface and thus select specific orientations of the molecule. Immobilizing the sample to a carbon, graphene or graphene oxide support substrate reduces interactions at the air-water interface. In contrast to the air-water interface, graphene oxide is hydrophilic, and thus will interact with different surfaces of separase-securin, promoting different orientations.

Electron microscopy data collection

Purified separase-securin complexes from *C. elegans* and human were applied to graphene oxide covered gold 300 square mesh Quantifoil R1.2/1.3 holey-carbon grids (Quantifoil Micro Tools GmbH) at a concentration of ~100 nM (waiting time 30s, blotting time 8s) and

flash frozen in liquid ethane using a custom fabricated manual plunger at 4 °C. *C. elegans* separase specimens were specimens were imaged manually on an FEI Titan Krios electron microscope operating at 300 kV accelerating voltage. Zero-energy-loss micrographs were recorded using a Gatan K2-Summit direct electron detector executed in super-resolution counting mode at the end of a Gatan GIF-Quantum energy filter with a slit width of 20 eV. The calibrated magnification was 34,965 corresponding to a pixel size of 1.43 Å and images were collected at a dose rate of ~2.5 electrons/Å^2/s. Exposures of 16 seconds were dose-fractionated into 20 movie frames with a total dose of ~40 electrons per Å^2. Defocus values in the final data set ranged from -1.0 to -3.3 μm. Automated data acquisition applying the same exposure time and total dose as described for the *C. elegans* separase-securin complex was used for data collection of the human separase-securin complex at Diamond Light Source (DLS) with a calibrated magnification of 47,619 that corresponds to a pixel size of 1.05 Å.

Image processing

Super resolution micrograph movies with a pixel size of 0.715 Å were binned to 1.43 Å. Micrograph movie frame stacks were first aligned using MOTIONCORR 45 before further processing. The contrast transfer function (CTF) parameters were determined using GCTF 46 and RELION 47 was used for most other image processing steps. Initial particle picking was performed using e2boxer.py in EMAN2 (ref. 48) employing only a subset of the data set and particles were extracted applying a 180 pixel * 180 pixel box. Reference-free 2D classification yielded into initial 2D classes that were subsequently used as references (low-pass filter of 20 Å was applied to avoid reference bias) for automatic particle picking 49. A high-pass filter of 400 Å with a 50 Å width of the raised cosine on the high-pass filter edge was applied to all micrographs to correct for the ice gradient present on most of the micrographs in order to reduce false positive picking of particles. In total 2.4 million particles were picked from 2,793 micrographs and extracted from original unmodified micrographs. Reiterative reference-free two-dimensional class averaging and strict selection of classes that showed distinct/strong structural features resulted into a particle subset of 665,331 particles. An *ab initio* 3D reconstruction was created using SIMPLE-PRIME 50 and used as an initial model for a first 3D refinement. Correction of beam-induced motion of individual particles and B-factor weighting of single frames to treat radiation damage problems were performed in the particle polishing step 51 in RELION. Auto-refinement of polished particles with a soft mask (with 5-pixel fall-off) around the entire molecule led to a density map of 4.2 Å resolution. This particle subset was subjected to two rounds of three-dimensional classifications to separate structural heterogeneity and dispose of remaining bad particles (see Supplementary Fig. 9). In a final step all micrographs with a resolution lower than 4.0 Å according to the resolution estimation of GCTF were discarded, which resulted in a final data set of 103,696 particles that refined to a map with the resolution of 3.8 Å. All resolution estimations are derived from Fourier shell correlation (FSC) calculations between reconstructions from two independently refined half-sets and reported resolutions are based on the FSC = 0.143 criterion 52,53. Local resolution was estimated using ResMap 54. Images collected at the DLS were collected in counting mode and processed as described for the *C. elegans* data set with the exception of a 240 * 240 pixel box size due to larger particle size. Auto-refinement of particles with a soft mask (with 5-pixel fall-off) around the entire

molecule led to a density map of 6.8 Å resolution. This resolution estimation is likely overestimated due to the strong preferred orientation of particles.

Model building and refinement of the *Ce* separase-securin complex

Ab initio modeling of the entire *Ce* separase-securin complex was performed in COOT 55. A recently published crystal structure of the C-terminal lobe of the *Chaetomium thermophilum* separase 25 was fitted into the density using Chimera 56 and used as a template and validation tool for modeling the SPD. The final model of separase lacks the N-terminal ten residues, two long unstructured loop regions (insert-1 and insert-2) present in the α-solenoid domain (residues 391-446 and residues 590-626) as well as the C-terminal 122 residues that are predicted to be unstructured and for which no density could be observed. The model was refined using Refmac v.5.8 (ref. 57) with a weight and PHENIX 58. Secondary structure restrains were created by PROSMART 59.

Structure-based sequence alignment of separase TPR domains

The N-terminal sequence of human separase (residues 1 to 1692, N-terminal to the separase protease domain) was analysed for predicted secondary structure elements and disordered regions using PHYRE2 60. This indicated an α-helical segment interspersed with two predicted disordered regions (residues 1070-1040 and 1307-1561). The positions of these two disordered regions approximately matched Insert-1 and Insert-2 of *C. elegans* separase (390-442 and 597-618). Residues 1-390 of *C. elegans* separase were aligned with residues 651-1070 of human separase, based on matching predicted α-helices of human separase with observed α-helices of *C. elegans* separase and also guided by a published multiple sequence alignment of part of the N-terminal domain of separase 27. Residues 442-597 and 618-700 of *C. elegans* separase aligned with residues 1140-1307 and 1561-1641 of human separase, respectively.

Supplementary Material

Refer to Web version on PubMed Central for supplementary material.

Acknowledgments

This work was funded by the Medical Research Council (MC_UP_1201/6 to DB and MC_UP_A025_1013 to SHWS), a Cancer Research UK grant (C576/A14109) to D.B., a Long Term EMBO Fellowships to A.B. (ALTF 79-2014) and T.G.M. (ALTF 1229-2013) and H2020 Marie-Curie Fellowships to A.B. (657725) and T.G.M. (657990). We thank members of the Barford group for helpful discussions, T. Tischer for helpful suggestions and support. C. Savva, S. Chen and G. McMullan for maintaining EM facilities; J. Grimmett and T. Darling for computing and P. Emsley for constant support with COOT. We acknowledge Diamond for access and support of the Cryo-EM facilities at the UK national electron bio-imaging centre (eBIC), proposal EM13708, funded by the Wellcome Trust, MRC and BBSRC.

References

1. Uhlmann F, Wernic D, Poupart MA, Koonin EV, Nasmyth K. Cleavage of cohesin by the CD clan protease separin triggers anaphase in yeast. Cell. 2000; 103:375–86. [PubMed: 11081625]
2. Waizenegger IC, Hauf S, Meinke A, Peters JM. Two distinct pathways remove mammalian cohesin from chromosome arms in prophase and from centromeres in anaphase. Cell. 2000; 103:399–410. [PubMed: 11081627]

3. Hauf S, Waizenegger IC, Peters JM. Cohesin cleavage by separase required for anaphase and cytokinesis in human cells. Science. 2001; 293:1320–3. [PubMed: 11509732]
4. Santaguida S, Amon A. Short- and long-term effects of chromosome mis-segregation and aneuploidy. Nat Rev Mol Cell Biol. 2015; 16:473–85. [PubMed: 26204159]
5. Kamenz J, Hauf S. Time To Split Up: Dynamics of Chromosome Separation. Trends Cell Biol. 2017; 27:42–54. [PubMed: 27567180]
6. Ciosk R, et al. An ESP1/PDS1 complex regulates loss of sister chromatid cohesion at the metaphase to anaphase transition in yeast. Cell. 1998; 93:1067–76. [PubMed: 9635435]
7. Uhlmann F, Lottspeich F, Nasmyth K. Sister-chromatid separation at anaphase onset is promoted by cleavage of the cohesin subunit Scc1. Nature. 1999; 400:37–42. [PubMed: 10403247]
8. Zou H, McGarry TJ, Bernal T, Kirschner MW. Identification of a vertebrate sister-chromatid separation inhibitor involved in transformation and tumorigenesis. Science. 1999; 285:418–22. [PubMed: 10411507]
9. Sanchez-Puig N, Veprintsev DB, Fersht AR. Human full-length Securin is a natively unfolded protein. Protein Sci. 2005; 14:1410–8. [PubMed: 15929994]
10. Csizmok V, Felli IC, Tompa P, Banci L, Bertini I. Structural and dynamic characterization of intrinsically disordered human securin by NMR spectroscopy. J Am Chem Soc. 2008; 130:16873–9. [PubMed: 19053469]
11. Hellmuth S, et al. Positive and negative regulation of vertebrate separase by Cdk1-cyclin B1 may explain why securin is dispensable. J Biol Chem. 2015; 290:8002–10. [PubMed: 25659430]
12. Jallepalli PV, et al. Securin is required for chromosomal stability in human cells. Cell. 2001; 105:445–57. [PubMed: 11371342]
13. Nagao K, Adachi Y, Yanagida M. Separase-mediated cleavage of cohesin at interphase is required for DNA repair. Nature. 2004; 430:1044–8. [PubMed: 15329725]
14. Hornig NC, Knowles PP, McDonald NQ, Uhlmann F. The dual mechanism of separase regulation by securin. Curr Biol. 2002; 12:973–82. [PubMed: 12123570]
15. Holland AJ, Taylor SS. Cyclin-B1-mediated inhibition of excess separase is required for timely chromosome disjunction. J Cell Sci. 2006; 119:3325–36. [PubMed: 16868023]
16. Bachmann G, et al. A closed conformation of the Caenorhabditis elegans separase-securin complex. Open Biol. 2016; 6
17. Stemmann O, Zou H, Gerber SA, Gygi SP, Kirschner MW. Dual inhibition of sister chromatid separation at metaphase. Cell. 2001; 107:715–26. [PubMed: 11747808]
18. Gorr IH, Boos D, Stemmann O. Mutual inhibition of separase and Cdk1 by two-step complex formation. Mol Cell. 2005; 19:135–41. [PubMed: 15989971]
19. Cohen-Fix O, Peters JM, Kirschner MW, Koshland D. Anaphase initiation in Saccharomyces cerevisiae is controlled by the APC-dependent degradation of the anaphase inhibitor Pds1p. Genes Dev. 1996; 10:3081–93. [PubMed: 8985178]
20. Funabiki H, et al. Cut2 proteolysis required for sister-chromatid seperation in fission yeast. Nature. 1996; 381:438–41. [PubMed: 8632802]
21. Yamamoto A, Guacci V, Koshland D. Pds1p, an inhibitor of anaphase in budding yeast, plays a critical role in the APC and checkpoint pathway(s). J Cell Biol. 1996; 133:99–110. [PubMed: 8601617]
22. Sullivan M, Hornig NC, Porstmann T, Uhlmann F. Studies on substrate recognition by the budding yeast separase. J Biol Chem. 2004; 279:1191–6. [PubMed: 14585836]
23. Alexandru G, Uhlmann F, Mechtler K, Poupart MA, Nasmyth K. Phosphorylation of the cohesin subunit Scc1 by Polo/Cdc5 kinase regulates sister chromatid separation in yeast. Cell. 2001; 105:459–72. [PubMed: 11371343]
24. Viadiu H, Stemmann O, Kirschner MW, Walz T. Domain structure of separase and its binding to securin as determined by EM. Nat Struct Mol Biol. 2005; 12:552–3. [PubMed: 15880121]
25. Lin Z, Luo X, Yu H. Structural basis of cohesin cleavage by separase. Nature. 2016; 532:131–4. [PubMed: 27027290]

Europe PMC Funders Author Manuscripts

26. Pantelic RS, Meyer JC, Kaiser U, Baumeister W, Plitzko JM. Graphene oxide: a substrate for optimizing preparations of frozen-hydrated samples. J Struct Biol. 2010; 170:152–6. [PubMed: 20035878]
27. Katis VL, et al. Rec8 phosphorylation by casein kinase 1 and Cdc7-Dbf4 kinase regulates cohesin cleavage by separase during meiosis. Dev Cell. 2010; 18:397–409. [PubMed: 20230747]
28. Hellmuth S, et al. Human chromosome segregation involves multi-layered regulation of separase by the peptidyl-prolyl-isomerase Pin1. Mol Cell. 2015; 58:495–506. [PubMed: 25921067]
29. Waizenegger I, Gimenez-Abian JF, Wernic D, Peters JM. Regulation of human separase by securin binding and autocleavage. Curr Biol. 2002; 12:1368–78. [PubMed: 12194817]
30. Zou H, Stemman O, Anderson JS, Mann M, Kirschner MW. Anaphase specific auto-cleavage of separase. FEBS Lett. 2002; 528:246–50. [PubMed: 12297314]
31. Holland AJ, Bottger F, Stemmann O, Taylor SS. Protein phosphatase 2A and separase form a complex regulated by separase autocleavage. J Biol Chem. 2007; 282:24623–32. [PubMed: 17604273]
32. Sun Y, et al. Separase is recruited to mitotic chromosomes to dissolve sister chromatid cohesion in a DNA-dependent manner. Cell. 2009; 137:123–32. [PubMed: 19345191]
33. McLuskey K, Mottram JC. Comparative structural analysis of the caspase family with other clan CD cysteine peptidases. Biochem J. 2015; 466:219–32. [PubMed: 25697094]
34. Nagao K, Yanagida M. Securin can have a separase cleavage site by substitution mutations in the domain required for stabilization and inhibition of separase. Genes Cells. 2006; 11:247–60. [PubMed: 16483313]
35. Buonomo SB, et al. Disjunction of homologous chromosomes in meiosis I depends on proteolytic cleavage of the meiotic cohesin Rec8 by separin. Cell. 2000; 103:387–98. [PubMed: 11081626]
36. Sullivan M, Lehane C, Uhlmann F. Orchestrating anaphase and mitotic exit: separase cleavage and localization of Slk19. Nat Cell Biol. 2001; 3:771–7. [PubMed: 11533655]
37. Matsuo K, et al. Kendrin is a novel substrate for separase involved in the licensing of centriole duplication. Curr Biol. 2012; 22:915–21. [PubMed: 22542101]
38. Keusekotten K, et al. OTULIN antagonizes LUBAC signaling by specifically hydrolyzing Met1-linked polyubiquitin. Cell. 2013; 153:1312–26. [PubMed: 23746843]
39. Wickliffe KE, Lorenz S, Wemmer DE, Kuriyan J, Rape M. The mechanism of linkage-specific ubiquitin chain elongation by a single-subunit E2. Cell. 2011; 144:769–81. [PubMed: 21376237]
40. Huang Y, et al. Structural basis of caspase inhibition by XIAP: differential roles of the linker versus the BIR domain. Cell. 2001; 104:781–90. [PubMed: 11257231]
41. Riedl SJ, et al. Structural basis for the inhibition of caspase-3 by XIAP. Cell. 2001; 104:791–800. [PubMed: 11257232]
42. Zhang N, et al. Overexpression of Separase induces aneuploidy and mammary tumorigenesis. Proc Natl Acad Sci U S A. 2008; 105:13033–8. [PubMed: 18728194]
43. Mukherjee M, et al. Overexpression and constitutive nuclear localization of cohesin protease Separase protein correlates with high incidence of relapse and reduced overall survival in glioblastoma multiforme. J Neurooncol. 2014; 119:27–35. [PubMed: 24792645]
44. Zhang Z, Yang J, Barford D. Recombinant expression and reconstitution of multiprotein complexes by the USER cloning method in the insect cell-baculovirus expression system. Methods. 2016; 95:13–25. [PubMed: 26454197]
45. Li X, et al. Electron counting and beam-induced motion correction enable near-atomic-resolution single-particle cryo-EM. Nat Methods. 2013; 10:584–90. [PubMed: 23644547]
46. Zhang K. Gctf: Real-time CTF determination and correction. J Struct Biol. 2016; 193:1–12. [PubMed: 26592709]
47. Scheres SH. RELION: implementation of a Bayesian approach to cryo-EM structure determination. J Struct Biol. 2012; 180:519–30. [PubMed: 23000701]
48. Tang G, et al. EMAN2: an extensible image processing suite for electron microscopy. J Struct Biol. 2007; 157:38–46. [PubMed: 16859925]
49. Scheres SH. Semi-automated selection of cryo-EM particles in RELION-1.3. J Struct Biol. 2015; 189:114–22. [PubMed: 25486611]

50. Elmlund H, Elmlund D, Bengio S. PRIME: probabilistic initial 3D model generation for single-particle cryo-electron microscopy. Structure. 2013; 21:1299–306. [PubMed: 23931142]
51. Scheres SH. Beam-induced motion correction for sub-megadalton cryo-EM particles. Elife. 2014; 3:e03665. [PubMed: 25122622]
52. Scheres SH, Chen S. Prevention of overfitting in cryo-EM structure determination. Nat Methods. 2012; 9:853–4. [PubMed: 22842542]
53. Rosenthal PB, Henderson R. Optimal determination of particle orientation, absolute hand, and contrast loss in single-particle electron cryomicroscopy. J Mol Biol. 2003; 333:721–45. [PubMed: 14568533]
54. Kucukelbir A, Sigworth FJ, Tagare HD. Quantifying the local resolution of cryo-EM density maps. Nat Methods. 2014; 11:63–5. [PubMed: 24213166]
55. Emsley P, Cowtan K. Coot: model-building tools for molecular graphics. Acta Crystallogr D Biol Crystallogr. 2004; 60:2126–32. [PubMed: 15572765]
56. Yang Z, et al. UCSF Chimera, MODELLER, and IMP: an integrated modeling system. J Struct Biol. 2012; 179:269–78. [PubMed: 21963794]
57. Murshudov GN, et al. REFMAC5 for the refinement of macromolecular crystal structures. Acta Crystallogr D Biol Crystallogr. 2011; 67:355–67. [PubMed: 21460454]
58. Adams PD, et al. PHENIX: building new software for automated crystallographic structure determination. Acta Crystallogr D Biol Crystallogr. 2002; 58:1948–54. [PubMed: 12393927]
59. Nicholls RA, Fischer M, McNicholas S, Murshudov GN. Conformation-independent structural comparison of macromolecules with ProSMART. Acta Crystallogr D Biol Crystallogr. 2014; 70:2487–99. [PubMed: 25195761]
60. Kelley LA, Mezulis S, Yates CM, Wass MN, Sternberg MJ. The Phyre2 web portal for protein modeling, prediction and analysis. Nat Protoc. 2015; 10:845–58. [PubMed: 25950237]
61. Barton GJ. ALSCRIPT: a tool to format multiple sequence alignments. Protein Eng. 1993; 6:37–40. [PubMed: 8433969]

Europe PMC Funders Author Manuscripts

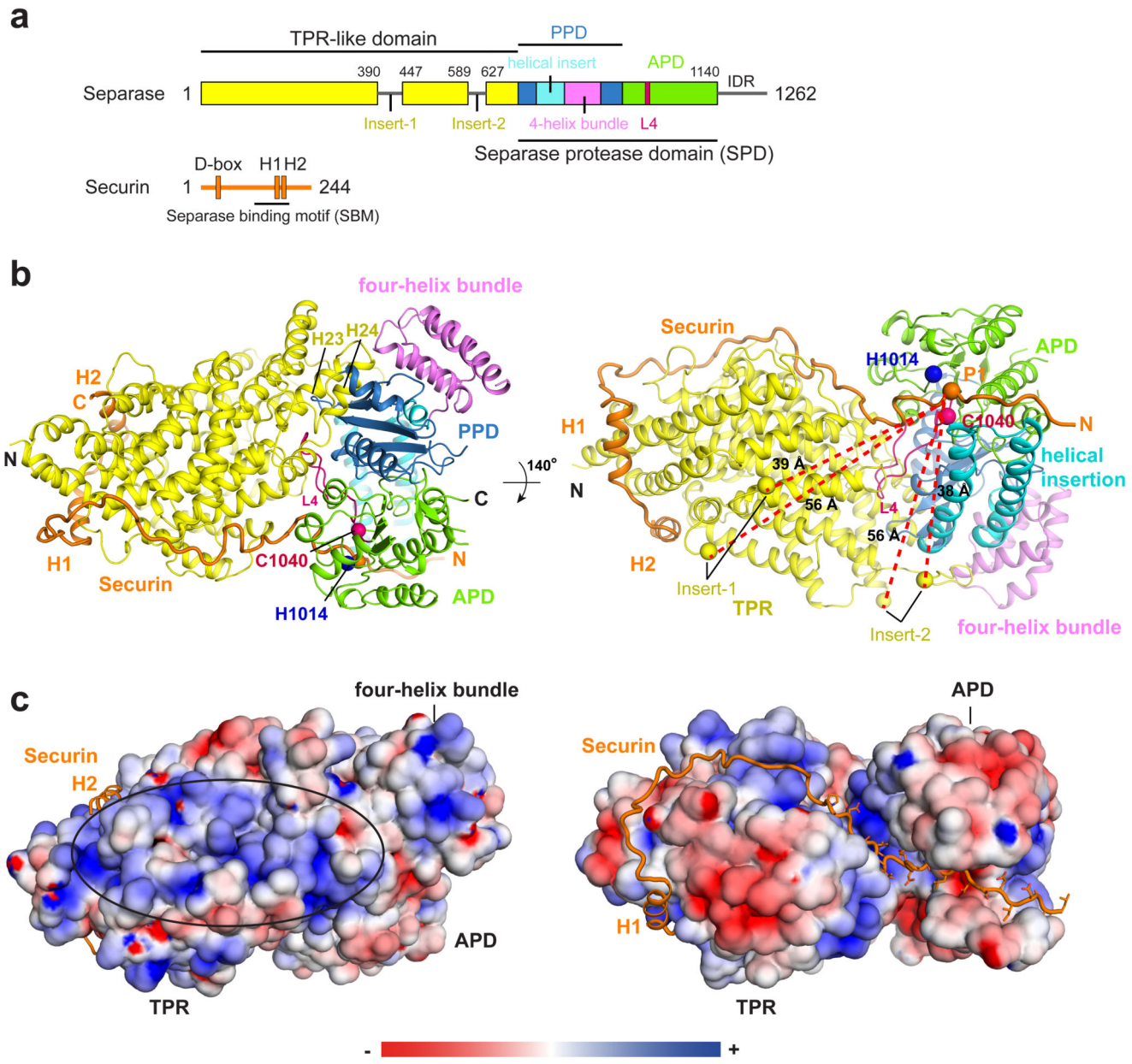

Figure 1. Overview of the *C. elegans* separase-securin complex.

a, Schematic of separase and securin**. b,** Two views of the separase-securin complex. The catalytic dyad of His1014 and Cys1040, and L4 loop indicate the catalytic site. The positions of Insert-1 and Insert-2 relative to the catalytic site (corresponding to the Cα-atom of the P1 Met of securin) are indicated as spheres. Distances between the insert boundaries and the Cα-atom of the P1 residue of securin ($Met126^{Sec}$) are shown. **c**, Two views of the molecular surface of separase showing electrostatic potential, with securin in stick representation. The positively charged surface is indicated (left).

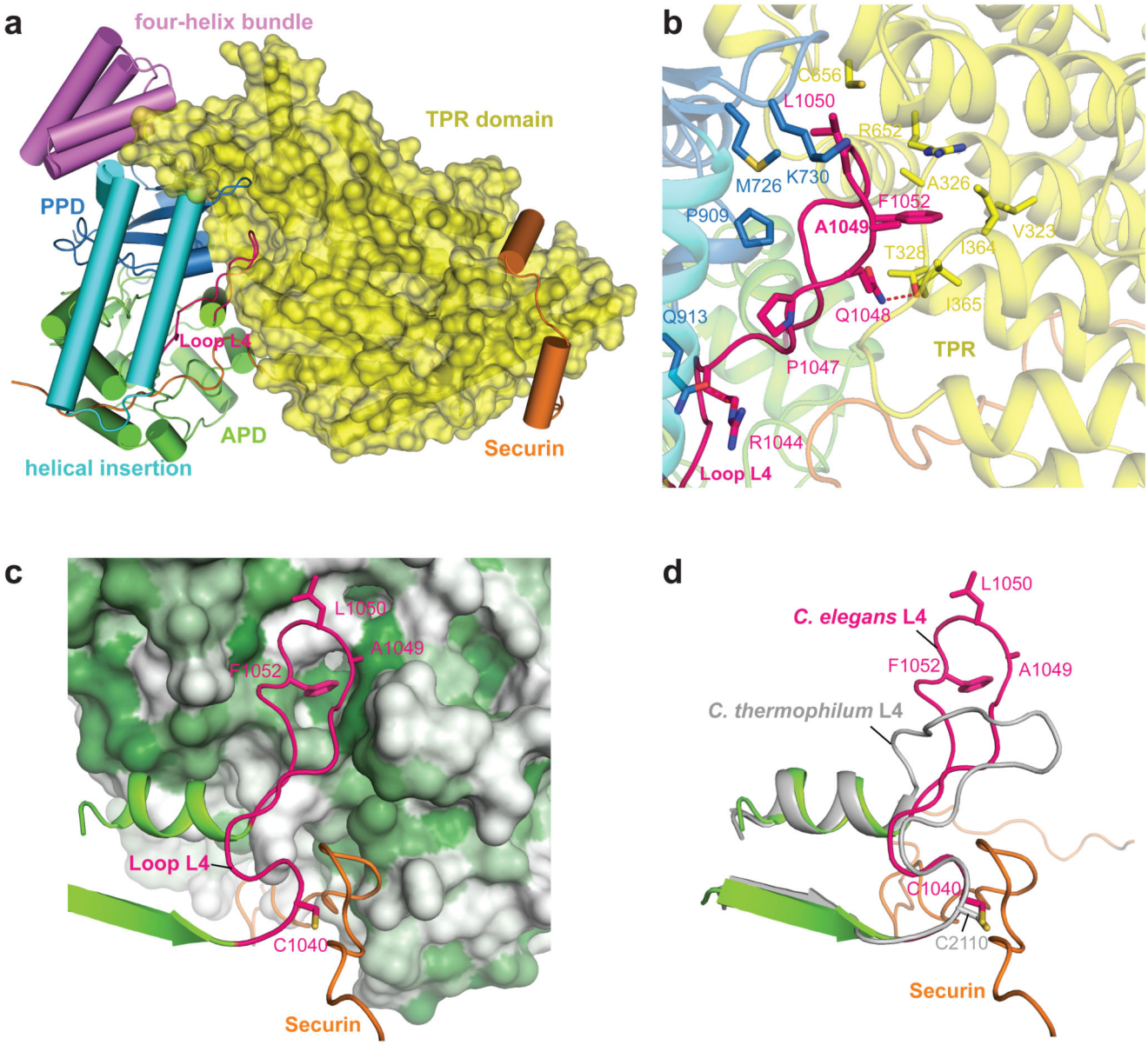

Figure 2. The α-solenoid domain stabilizes the L4 loop.

a, Overview of separase-securin showing the molecular surface of the separase α-solenoid domain. **b,** Details of the L4 loop interactions with the α-solenoid domain. **c,** View of the L4 loop docking into the L4-loop binding pocket of the α-solenoid domain shown as a hydrophobic surface colour-ramped from white to green with increasing hydrophobicity. **d,** The L4 loops of *Ce*SPD and *Ct*SPD adopt an active conformation, with differences confined to the tip of the loop. Securin contacts the L4 loop.

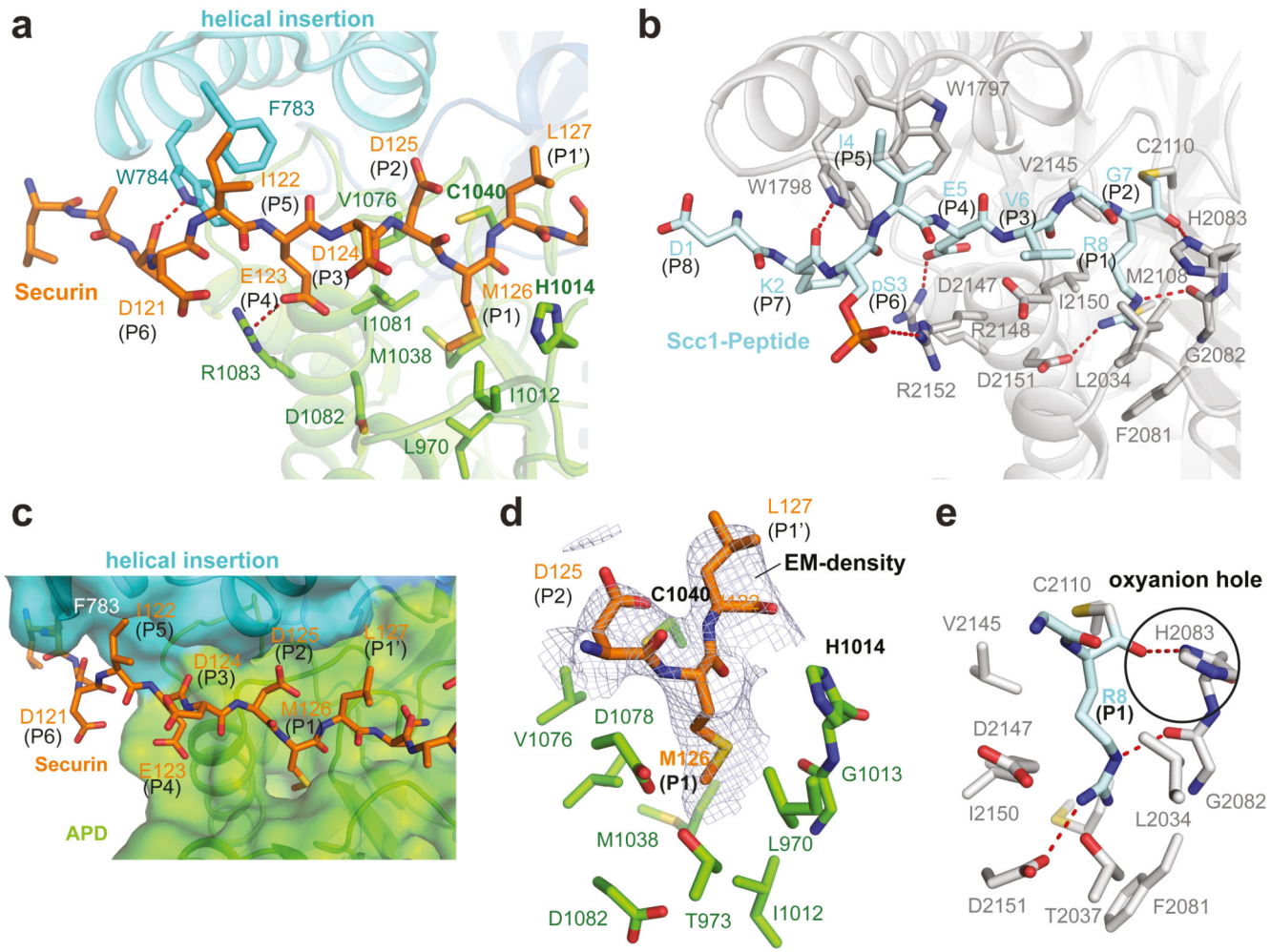

Figure 3. The interactions of the securin pseudo-substrate motif with separase resemble Scc1.

a, Securin pseudo-substrate motif at the *Ce*SPD. **b**, Scc1-mimicking peptide at *Ct*SPD 25. **c**, The molecular surface of *Ce* separase showing the securin pseudo-substrate sequence engaging the peptide-substrate binding site of separase. **d**, Details of the Met126(P1) residue at the P1-binding site and its corresponding EM density. **e**, P1 Arg of the Scc1-mimicking peptide at the P1-site of *Ct*SPD showing the oxyanion hole formed from the catalytic His2083 (from ref. 25). The guanidinium side chain of the P1-Arg residue donates a hydrogen bond to the main-chain carbonyl of Gly2082, positioning the imidazole side chain of His2083 to create the oxyanion hole and donate a hydrogen bond to the main-chain carbonyl of Arg(P1). In contrast, Met126(P1) of *C. elegans* Scc1 widens the P1-binding pocket *C. elegans* separase such that the main-chain of Gly1012 and side chain of His1014 (equivalent to Gly2082 and His2083, respectively of *Ct*SPD) are displaced by ~2 Å.

Europe PMC Funders Author Manuscripts

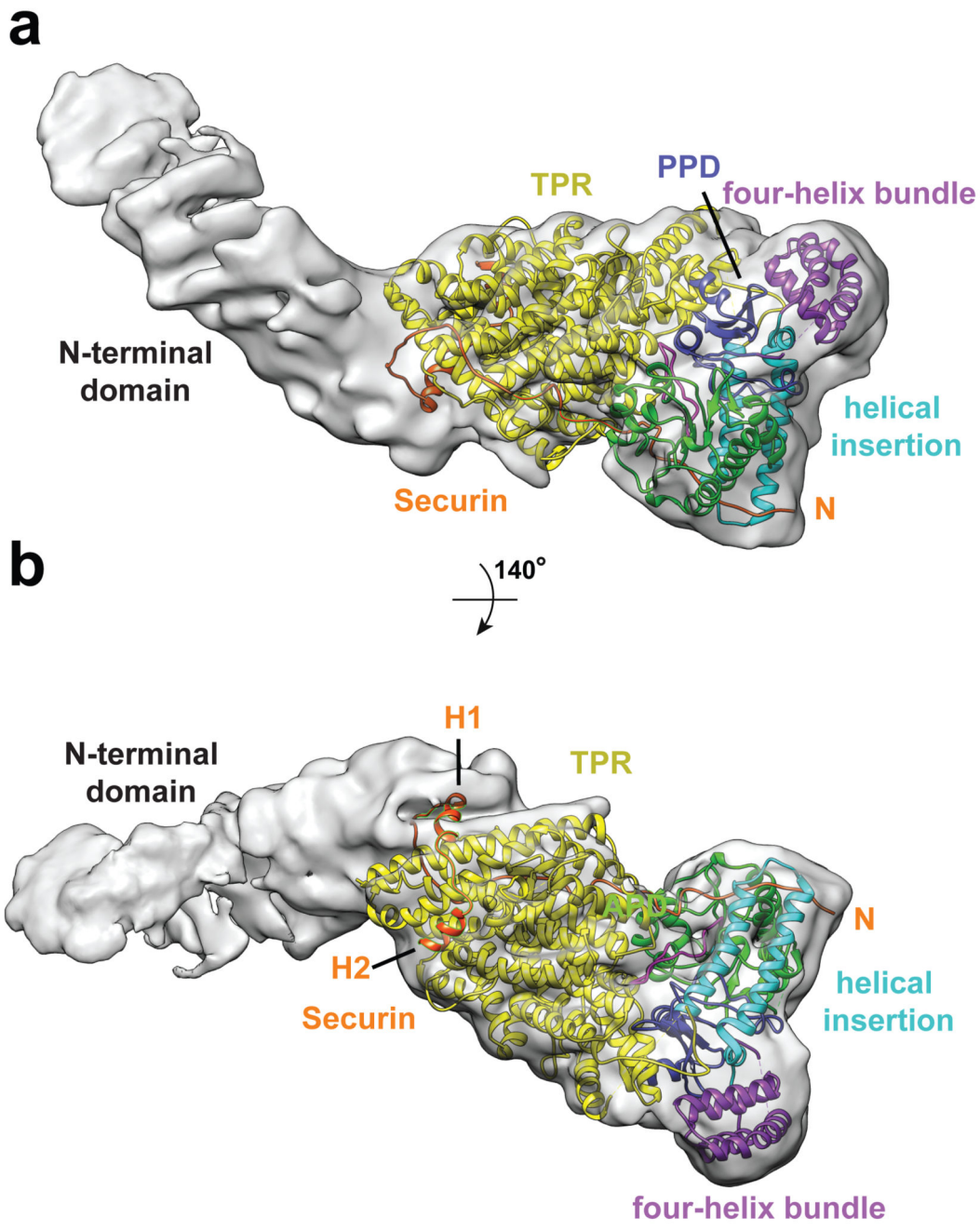

Figure 4. Cryo-EM reconstruction of human separase-securin complex.

a and **b**, Two views showing the cryo-EM density as a transparent molecular envelop with the coordinates of *C. elegans* separase-securin fitted to the map as a rigid body. Colour-code according to Fig. 1.

Table 1

EM data collection and processing and structure refinement statistics.

	***Ce*Separase-securin (EMD-3583, PDB 5MZ6)**	***Hs*Separase-securin (EMD-3584)**
Data collection		
Microscope	FEI Titan Krios	FEI Titan Krios
Voltage (kV)	300	300
Electron dose (e Å $^{-2}$)	40	40
Detector	Gatan K2 Summit	Gatan K2 Summit
Pixel size (Å)	1.43	1.05
Defocus Range (μm)	1.0-3.0	1.0-3.0
Reconstruction (Relion)		
Particles	103,696	152,374
Box size (pix)	180	240
Accuracy of rotations (°)	1.960	3.283
Accuracy of translations (pix)	0.492	1.994
Map sharpening B-factor (Å^2)	-130	
Final resolution (Å)	3.8	6.8
Model composition		
Protein residues	1097	
Refinement		
Resolution (Å)	3.8	
$FSC_{average}$	0.82	
R factor	36.53	
R.m.s deviations		
Bond lengths (Å)	0.007	
Bong angles (°)	1.012	
Validation[2]		
Clashscore, all atoms	11.12	
Rotamer outliers (%)	0.57	
Ramachandran plot		
Favoured (%)	93.73	
Allowed (%)	6.09	
Outliers (%)	0.18	
Disordered regions		
Separase	1-10, 391-446, 590-628, 894-899, 1095-1104, 1141-1262	
Securin	1-117, 193-244	
Side chains fitted (%)		
Separase (of ordered region)	96.3	
Securin (of ordered region)	84	